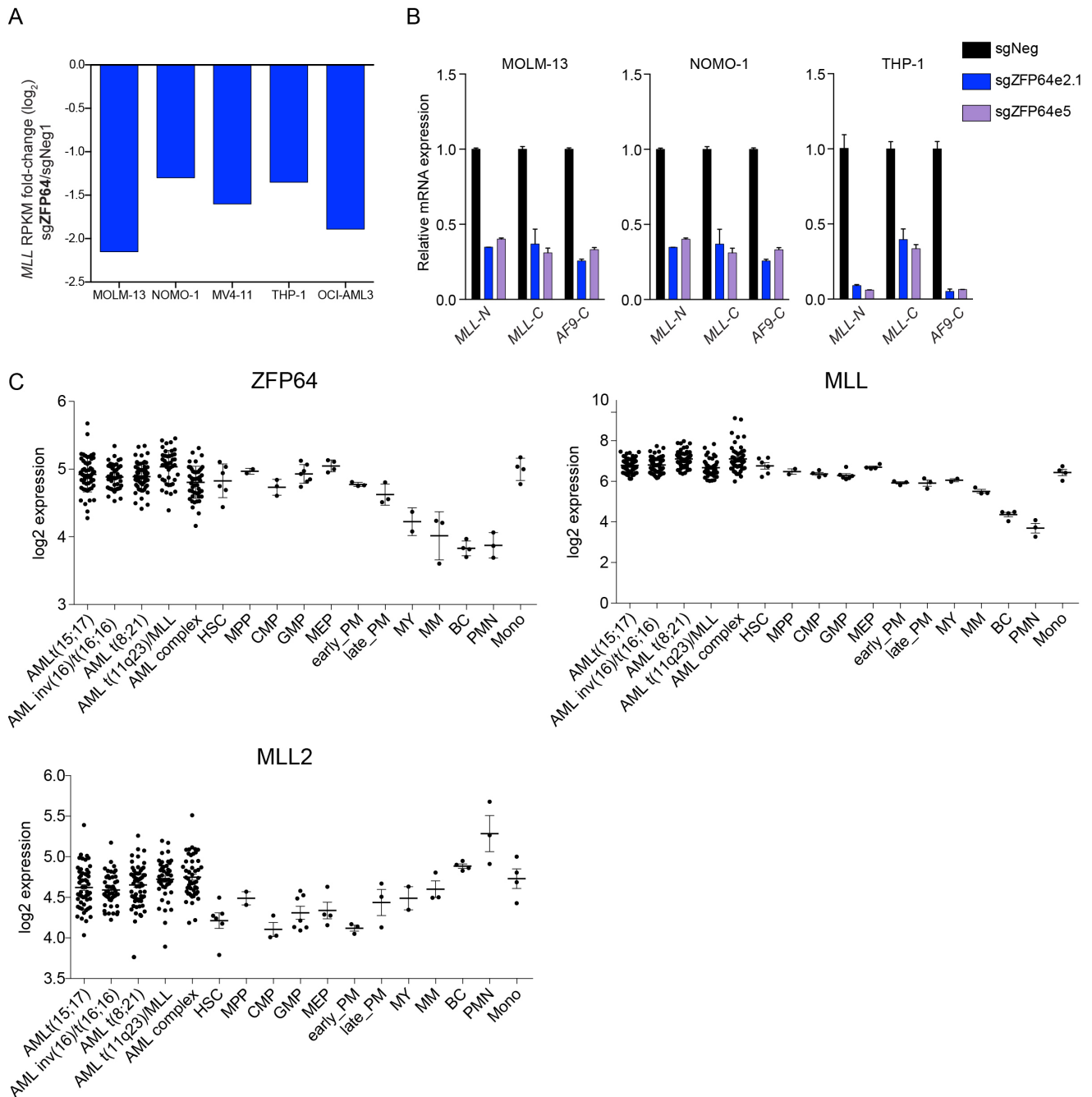


**Figure S1. CRISPR screening identifies ZFP64 as essential in MLL-rearranged leukemia. Related to Figure 1. (A)** Known genetic mutations in nine leukemia cell lines. **(B)** Illustration of MLL<sup>WT</sup> and MLL<sup>fusion</sup> protein domain architecture and location of MLL sgRNAs. **(C)** Left:

Bioluminescence imaging of NSG mice transplanted with luciferase<sup>+</sup>/Cas9<sup>+</sup> MOLM-13 cells transduced with either Neg1 or ZFP64 targeting sgRNAs. Irradiated mice were tail vein injected with 500,000 MOLM-13 cells and imaged on day 12 and 16 post-transplantation. Percentage of sgRNA<sup>+</sup>/GFP<sup>+</sup> MOLM-13 cells from pre-transplantation and terminally-diseased mice collected from bone marrow. Three mice were used for each cohort. All mice were sacrificed for flow cytometry analysis on day 16. **(D)** top: Design of CRISPR resistant ZFP64 cDNA and Western blot of ZFP64 expression in cells transduced with empty vector (EV) or the CRISPR-resistant ZFP64 cDNA (CR). Competition-based proliferation assay for rescue experiment in MOLM-13 after infection of CRISPR-resistant cDNA. **(E)** ZFP64 mRNA expression level (RPKM values from RNA-seq) across different cancer cell lines. **(F)** Western blotting of ZFP64 and HSC70 in MLL<sup>WT</sup> and MLL<sup>fusion</sup> leukemia cell lines. **(G)** ZFP64 mRNA expression level from the GTEx database across different human tissues. **(H)** Comparison of global mRNA changes after knock out of ZFP64 and MLL in MV4-11 and THP-1 (left two panels). or knock out ZFP64 and SIK3 or RUNX1 in MOLM-13 (right two panels). Plotted is the fold change based on two independent sgRNA targeting ZFP64, MLL, SIK3 and RUNX1 compared to a negative control sgRNA Neg1. **(I)** Flow cytometry analysis of Mac-1 (top) and c-Kit (bottom) cell surface expression on day 8 post-infection with the indicated sgRNAs expressed in MOLM-13 cells. All bar graphs represent the mean  $\pm$  SEM.



Prediction software: <http://zf.princeton.edu>. **(C)** Overlap of ZFP64 binding peaks obtained by ChIP-seq using endogenous or Flag-tagged protein in NOMO-1. **(D)** Density plot showing endogenous ZFP64 and FLAG-ZFP64 binding intensities around the summit of 3,423 high confidence overlapped ZFP64 peaks in NOMO-1 cells. **(E)** Overlap of ZFP64 peaks with histone marks or Pol II in MOLM-13 cells, which were datasets obtained from the indicated GEO accessions. **(F)** Sequencing depth normalized ChIP-seq pileup tracks showing ZFP64 and H3K27ac enrichment at the *HOXA* cluster in MOLM-13 and NOMO-1 cells. **(G)** ZFP64 motif counts and distribution at ZFP64 peaks identified in the vicinity of the seven ZFP64 target genes identified in Figure 2F.



**Figure S3. ZFP64 maintains *MLL* expression via promoter activation. Related to Figure 3. (A)** RNA-seq analysis evaluating *MLL* mRNA levels after ZFP64 sgRNA transduction in the indicated cell lines compared to a control sgRNA. **(B)** RT-PCR analysis of *MLL* or *AF9* exons regions in the indicated *MLL*-*AF9* leukemia cell lines after knock out ZFP64. RT-PCR primers were designed to detect an N-terminal region of *MLL* (*MLL*-N, found on *MLL*<sup>fusion</sup> and *MLL*<sup>WT</sup>), a C-terminal region of *MLL* (*MLL*-C, found only on *MLL*<sup>WT</sup>), and the C-terminus of *AF9* (*AF9*-C, found on *MLL*<sup>fusion</sup> and *AF9*<sup>WT</sup>). GAPDH is used as normalization control. Primer sequences are provided in Table S2. (n=3) **(C)** ZFP64, *MLL*, or *MLL2*/*KMT2B* mRNA expression within human leukemia patient samples or from purified normal human hematopoietic cells. Data was retrieved from BloodSpot. (<http://servers.binf.ku.dk/bloodspot/>). Abbreviations: HSC, Hematopoietic stem cell; MPP, Multipotential progenitors; CMP, Common myeloid progenitor cell; GMP, Granulocyte monocyte progenitors; MEP, Megakaryocyte-erythroid progenitor cell; early\_PM, Early Promyelocyte; late\_PM,

Late Promyelocyte; MY, Myelocyte; MM, Metamyelocytes; BC, Band cell; PMN, Polymorphonuclear cells; Mono, Monocytes. All bar graphs represent the mean  $\pm$  SEM.

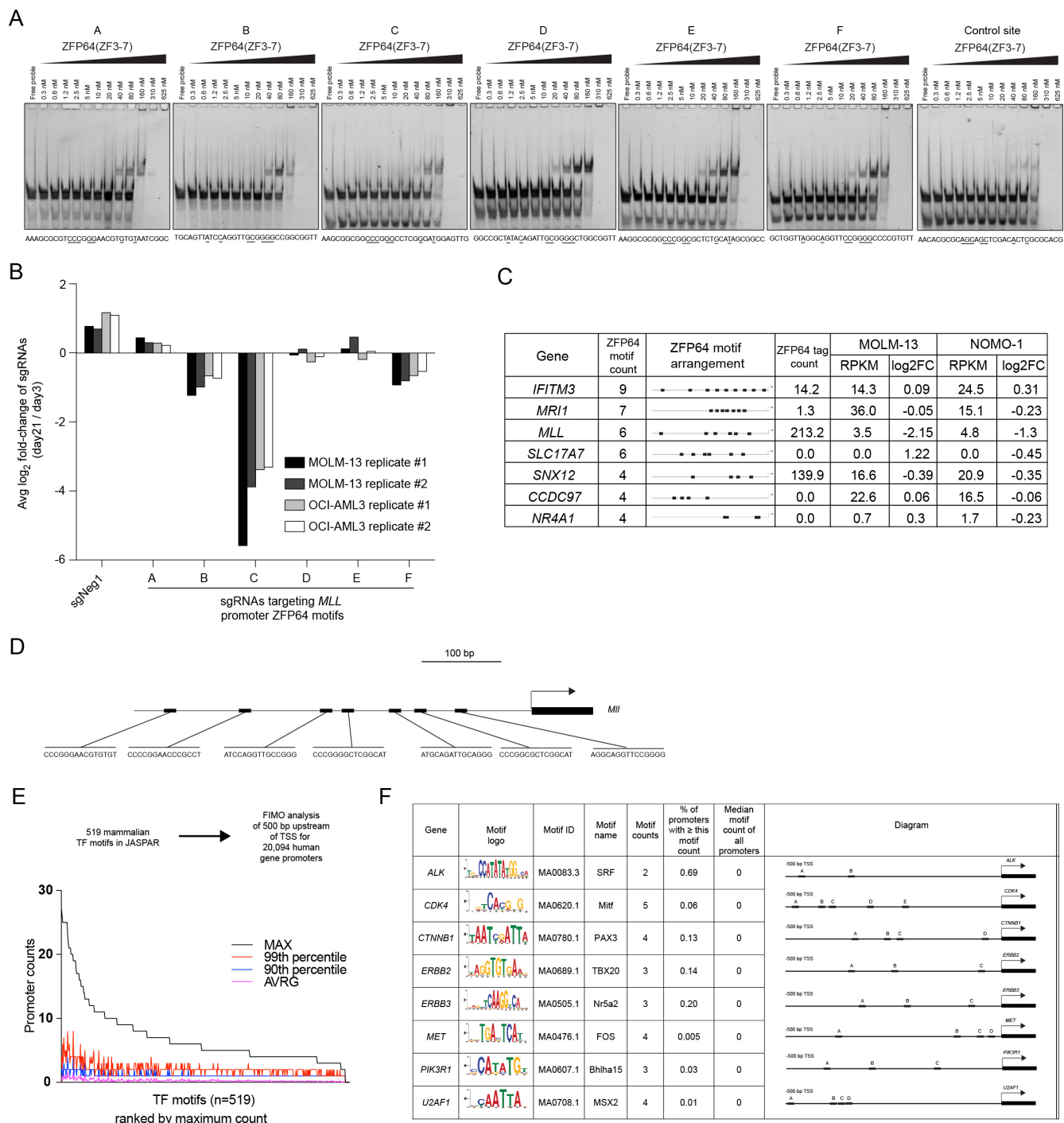


**Figure S4. An exceptional density of ZFP64 motifs at the *MLL* promoter. Related to Figure 4. (A)** EMSA assays showing the binding activity of recombinant ZFP64 (ZF3-7) to the six predicted ZFP64 motifs present in *MLL* promoter or to a control site. **(B)** CRISPR tiling experiment of the *MLL* promoter evaluating effect of indel mutagenesis in the vicinity of each ZFP64 motif on cell growth. ~10 sgRNAs were designed in the vicinity of each motif, which were pooled and subjected to a negative selection CRISPR screen in Cas9<sup>+</sup> MOLM-13 cells or OCI-AML3 cells. Average fold-change of sgRNAs targeting each motifs over 18 days in culture was quantified by next-gen sequencing. **(C)** Evaluation of ZFP64 occupancy and changes in mRNA abundance following ZFP64 knockout among

the 7 promoters harboring exceptional density of ZFP64 motifs. **(D)** Distribution of ZFP64 binding motifs in the mouse *Mll* promoter, identified using FIMO ( $p < 10^{-4}$ ). **(E)** FIMO analysis that interrogates all vertebrate TF motifs in the JASPAR database ( $n=519$ ) at all human protein coding gene promoters. The motif counts at each promoter were calculated ( $p < 10^{-4}$ ) and plotted is the average, 90<sup>th</sup> percentile, 99<sup>th</sup> percentile, and the maximum motif counts for each TF. **(F)** Using the analysis in (E), several human oncogene promoters were identified that possess motif counts that are in the top 1% among all human promoters in the genome.



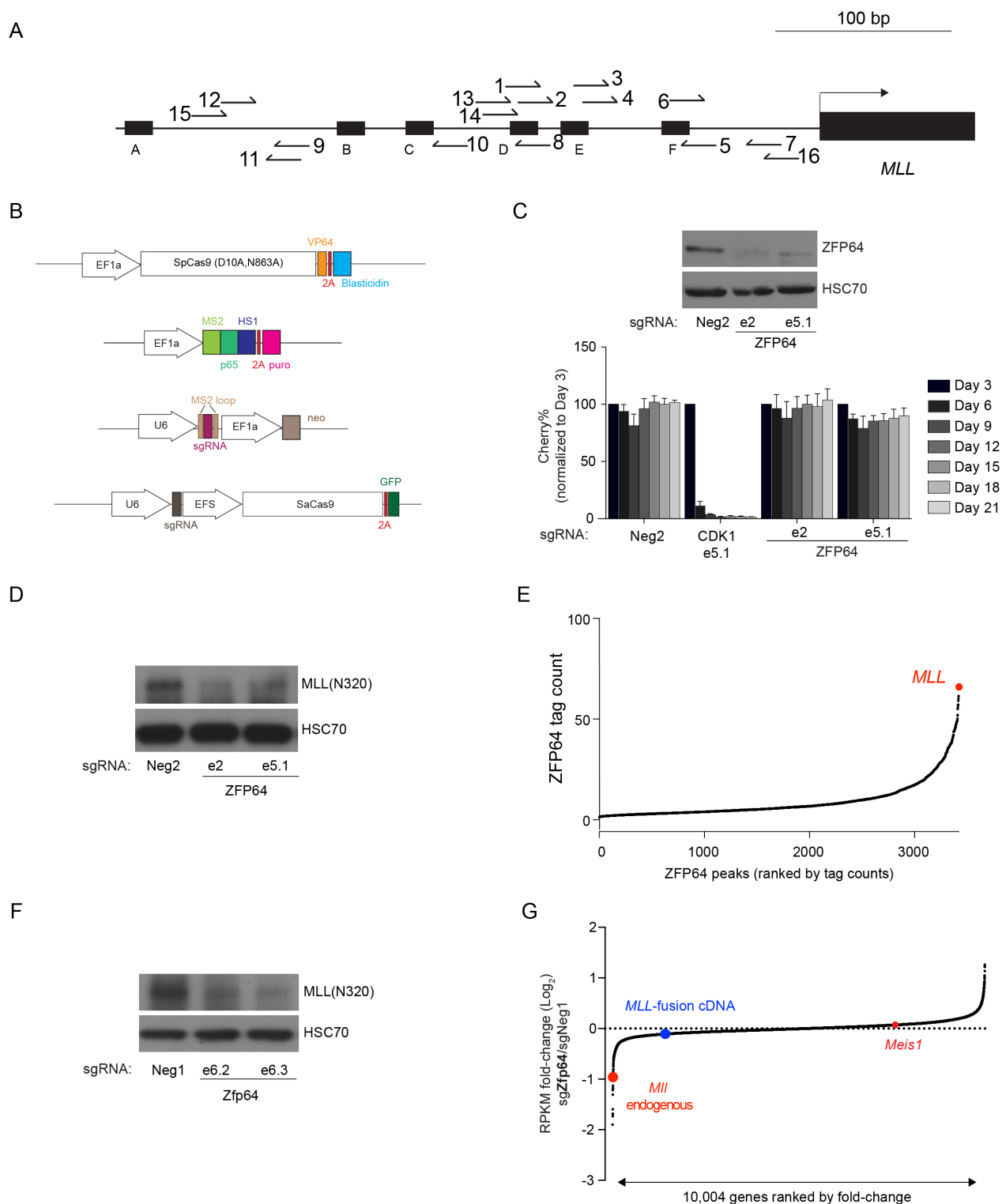


**Figure S5. MLL promoter activation is a critical function of ZFP64 underlying its essential function in MLL-fusion leukemia. Related to Figure 6. (A)** Schematic showing the position of sgRNAs used to activate endogenous *MLL* expression using CRISPR-activation relative to the position of six ZFP64 motifs. **(B)** Vectors used for dual CRISPR-activation/editing experiment. **(C)** Western blot and competition-based proliferation assay in MLL-AF9/FLT3<sup>ITD</sup> cells after transduction of sgRNAs targeting ZFP64. The presence of GFP in this engineered cell line led us to use sgRNA mCherry vector for this experiment. (n=3) **(D)** Western blotting of MLL in the human retroviral MLL-

AF9/Nras<sup>G12D</sup> AML cell line after ZFP64 sgRNA transduction. **(E)** Ranking of ZFP64 occupied sites in human retroviral MLL-AF9/Nras<sup>G12D</sup> AML cells using ChIP-seq. The *MLL* promoter peak of ZFP64 is indicated. **(F)** Western blot of endogenous MLL<sup>WT</sup> in mouse retroviral MLL-AF9/Nras<sup>G12D</sup> AML cells after transduction of sgRNA targeting mouse *Zfp64*. **(G)** RNA-seq analysis of mouse retroviral MLL-AF9/Nras<sup>G12D</sup> AML cells after transduction with sgRNAs targeting *Zfp64*. To evaluate endogenous *Mll*, a custom transcript was inserted into the analysis representing the C-terminal portion of the mouse gene. To evaluate the MLL fusion cDNA, a custom transcript of the human *MLL* N-terminus was inserted into the analysis. All bar graphs represent the mean  $\pm$  SEM.